

PCCP

Accepted Manuscript



This is an *Accepted Manuscript*, which has been through the Royal Society of Chemistry peer review process and has been accepted for publication.

Accepted Manuscripts are published online shortly after acceptance, before technical editing, formatting and proof reading. Using this free service, authors can make their results available to the community, in citable form, before we publish the edited article. We will replace this *Accepted Manuscript* with the edited and formatted *Advance Article* as soon as it is available.

You can find more information about *Accepted Manuscripts* in the [Information for Authors](#).

Please note that technical editing may introduce minor changes to the text and/or graphics, which may alter content. The journal's standard [Terms & Conditions](#) and the [Ethical guidelines](#) still apply. In no event shall the Royal Society of Chemistry be held responsible for any errors or omissions in this *Accepted Manuscript* or any consequences arising from the use of any information it contains.

Dramatic activities of Vanadate Intercalated Bismuth Doped

LDH for solar light photocatalysis

Lagnamayee Mohapatra^[a,b] and K. M. Parida*^[a,c]

[^a] Academy of Scientific and Innovative Research, New Delhi

[^b] Advanced Materials Technology Department
CSIR-Institute of Minerals and Materials Technology
Bhubaneswar—751 013, Odisha (India)

[c] Department of Chemistry
SOA University
Bhubaneswar—751 030, Odisha (India)
Fax: +91-674-2350642;
E-mail: kulamaniparida@soauniversity.ac.in

**K.M. Parida, SOA University, Bhubaneswar-751 013,*

Fax: +91-674-2350642;

Tel. no: +91(0674) 2350635

E-mail: paridakulamani@yahoo.com, kulamaniparida@soauniversity.ac.in

ABSTRACT

To harvest solar energy efficiently, a series of Zn/Bi layered double hydroxide (LDH) photocatalyst with different molar ratios of Zn/Bi (2:1,3:1,4:1) has been synthesized by coprecipitation method at constant pH. All the Bi doped LDH samples displayed hydroxalite-like structure with interlayer carbonate, in which crystallinity decreases as the bismuth content increases. The Zn/Bi (4:1) LDH with small amount of bismuth in the brucite layer and possessing high crystallinity was further modified hydrothermally by intercalating decavanadate which showed high photochemical stability and photocatalytic activity for the degradation of different organic pollutants for practical applications under solar light irradiation. The structural integrity of the materials has been successfully characterized by studying their structural, morphological, electronic and optical properties by various physico-chemical techniques. The present study introduced an insight of oxo-bridged MMCT of the LDH established the Zn (II) - O - Bi (III) units resulted in the generation of superoxide radicals which is clearly observed by the EPR technique. The $\cdot\text{OH}$ radicals formed during photocatalysis was revealed by means of terephthalic acid fluorescence probe method. The photo electrochemical measurement confirmed the intercalated vanadate anion was crucial to obtain an optimal synergistic effect for the degradation of organic pollutants. The prolonged photogenerated charge lifetime and improved charge transfer capability were confirmed by time-resolved fluorescence emission spectra. Furthermore, a detailed mechanism for the enhanced photocatalytic activity was discussed.

Keywords: Layered double hydroxide, decavanadate, Interlayer space, Fluorescence probe method, EPR technique.

INTRODUCTION

In recent days, the use of layered double hydroxide (LDH) as active photo-catalysts has been receiving considerable attention over the layered metal oxides. LDHs, important anionic clays are generally expressed by the formula $[M^{2+}_{1-x}M^{3+}_x(OH)_2]^{x+} (A^{n-})_{x/n} \cdot nH_2O$, where M^{2+} and M^{3+} are the metal cations and A^{n-} is the interlayer anion.¹⁻² The host structures of LDH are based on brucite-like (Mg (OH)₂) layers of edge-sharing MO₆ octahedron surrounded by oxo bridges and hydroxyl groups. The positive charge on the layers is compensated by NO₃⁻, SO₄²⁻, Cl⁻ and CO₃²⁻ ions present in the interlayer. Owing to the specific structure, tunable composition and nanoscale size, LDH powdered materials have been widely used as catalysts or catalyst precursors, anion exchangers, photo-active materials and bioactive nanocomposites.³⁻⁵ Garcia et al. reported doped semiconductors based Zn-containing LDHs for photocatalytic water splitting.⁶ Taking into account the high photocatalytic efficiency and quantum yield of the Zn²⁺/M³⁺ LDH compounds for visible light-induced O₂ generation, our group studied a family of visible-light-responsive Zn²⁺/M³⁺ LDH (M=Cr,Fe,Y) materials that exhibits remarkable photocatalytic activity for the decomposition of pollutants in water.⁷⁻⁹ Furthermore, Wei's group reported a family of visible-light-responsive dispersed MO₆ materials for the decomposition of organic pollutants in water.¹⁰⁻¹¹ Lately, several ternary LDHs were successfully synthesized by our groups as potential materials towards the photocatalysis.¹²⁻¹⁴ Likewise, titanium-embedded layered double hydroxides, a highly efficient photocatalyst was also reported by Kang *et al.*¹⁵ Moreover, the poly-oxometallates intercalated LDHs are of significantly importance because it could influence the optical, electronic and magnetic properties. For example, three-dimensional ordered macro porous LDHs intercalated by decatungstate anions exhibit a higher photocatalytic activity than the standard plate-like counterparts.¹⁶ Now-a-days Bi-

based layered semiconductors have attracted much attention for photocatalysis like BiVO₄,¹⁷⁻¹⁹ BiWO₄,²⁰⁻²² BiFeO₃,²³ etc.

On the basis of the above studies, we are inspired and motivated to synthesize well-defined visible light active bismuth doped LDHs, intend for environmental application. In an attempt to lower the band-gap energy and minimize the recombination of photo induced charge carriers with promising results in terms of degradation time and degree of mineralization, our approach allows to synthesize decavanadate intercalated bismuth doped LDHs. It is worthy to note that the modified bismuth doped LDH exhibited higher photocatalytic activity than that of all the as prepared LDHs. To our best knowledge, as of now, this LDH as a photocatalytic material has not been reported. The possible mechanism of the photocatalytic activities of the as prepared LDHs were systematically studied on the basis of the crystal structure, electronic structure, morphology, electrochemical and fluorescence properties.

EXPERIMENTAL SECTION

Material preparation

All the reagents are of analytical grade and used directly without further purification. Zn/Bi LDH was synthesized by the co-precipitation method following a procedure similar to that reported in the literature.⁷ A solution of 200 mL containing Zn (NO₃)₂·6H₂O, and Bi (NO₃)₃·7H₂O with a desired Zn/Bi molar ratios of 2:1, 3:1, 4:1 (solution 1) and 0.1 M NaOH (solution 2) were added slowly under vigorous stirring at room temperature until the pH reached at 9.0. LDHs prepared with molar ratios 4:1, 3:1 and 2:1 are named ZB4, ZB3, ZB2 respectively. The suspension of ZB4 was then transferred into the Teflon coated stainless steel autoclave for hydrothermal treatment at 120 °C temperature for 10 h. After the hydrothermal treatment, the suspension was filtered and washed thoroughly with hot distilled water. The washed precipitate was dried in an oven at 80°C for 12 h, named as

ZB_{Hy}4 LDH. For vanadate intercalation, 0.05 M of NaVO₃ in 150 mL distilled water was added drop wise to the ZB_{Hy}4 LDH suspension (contains 4 g of solid). Before addition of the vanadate solution, the pH of the slurry suspension was adjusted to 4.5 with HCl (by an ELICO L1 612 pH meter), which was maintained all along the addition and stirring periods. The obtained solid was centrifuged and washed until no free vanadate remained, thus leading to a sample named ZBV_{Hy}4 LDH.²⁴

Structural and morphological characterization

All the prepared samples were identified by Powder X-ray diffraction (PXRD) patterns on a Rigaku XRD-600 diffractometer using Cu-K α radiation ($\lambda = 1.5418 \text{ \AA}$) with a step size of 0.02° and 4 second per scan. The crystal size was calculated with the Scherrer equation ($\Phi = K\lambda / \beta \cos \theta$), where Φ is the crystal size, K is usually taken as 0.94, λ is 0.154 nm, which is the wavelength of the X-ray radiation, β is the full width at half maximum intensity (FWHM), and θ is the Bragg angle in [\AA]. Transmission electron microscopic (TEM) images were obtained on a Philips TECHNAI G2 operated at 200 kV, in which specimens were prepared by dispersing the powdered samples in ethanol by sonication for 15 min and then drop-drying on a copper grid coated with carbon film. BET surface areas of the samples were analyzed by the multipoint N₂ adsorption–desorption method at liquid nitrogen temperature ($-196 \text{ }^\circ\text{C}$) by an ASAP 2020 (Micromeritics) instrument. Prior to the analysis, the samples were degassed at 110°C and 5×10^{-4} Torr for 5 h to evacuate the physically adsorbed moisture. The Fourier transform infrared (FTIR) spectra of the samples were recorded on a Varian FTIR spectrophotometer (FTS-800) at room temperature taking KBr as the reference in the range of $400\text{--}4000 \text{ cm}^{-1}$. The UV–vis diffuse reflectance spectra of the samples in the range 200–800 nm were recorded in a UV–vis spectrophotometer (Cary 100 model EL 96043181). Pellets of 2 mm thickness of boric acid powder were used as a standard for baseline correction and the spectra were recorded in a range 200–800 nm.

Photoluminescence spectra measurements were performed on Perkin-Elmer (LS 55) fluorescence spectrophotometer. Time-resolved photoluminescence (PL) spectra were measured at room temperature with a Fluoromax-4 spectro-fluorometer (HORIBA Scientific). For the photo electrochemical study, $ZB_{Hy}4$ LDH and $ZBV_{Hy}4$ LDH film electrodes were prepared by electrophoretic deposition by taking an iodine (30 mg) solution in acetone (30 mL) that contained 30 mg of powder photocatalyst. Two parallel fluorine-doped tin oxide-coated electrodes were immersed in the solution with a 10–15 mm separation and a 60 V bias was applied between them for 2 minutes under potentiostat control. The coated area was fixed at 1.5 cm and then dried. The photo electrochemical measurements were performed by using a potentiostat–galvanostat (Versastat 3, Princeton Applied Re-search) under illumination ($\lambda = 420$ nm). The current voltage was measured by using a conventional pyrex electrochemical cell that consisted of a prepared electrode as the working electrode, and a Pt electrode and an Ag/AgCl electrode were used as the counter and reference electrodes, respectively. The potential of the working electrode was controlled by a potentiostat. The cell was filled with an aqueous solution of Na_2SO_4 (0.1M), and the pH was adjusted to 6.5.

Photocatalytic experiment

Photocatalytic degradation of three common organic pollutants such as malachite green (MG), rhodamine 6G (RHG) and 4-chloro-2-nitro phenol (CNP) was investigated in the present investigation. MG, a widely used dye, was chosen as a representative, N-containing, hetero aromatic, cationic thiazine dye with the chemical formula: $C_{23}H_{25}ClN_2$. Rhodamine 6G (RHG) with chemical formula: $C_{28}H_{31}N_2O_3Cl$ is a chemically stable organic basic dye with different functional groups used to dye wool, cotton, silk and papers where brilliant shades of fluorescent effects are required. 4-chloro 2- nitro phenol (CNP) is a toxic and

bio-refractory chosen as a pollutant which can cause considerable damage to the ecosystem and human health. The structure of all pollutants is represented in Fig. S1.

For a typical photocatalytic experiment, 20 mg of catalyst were added to an aqueous solution of usually 20 mL of 80 ppm MG, RHG and CNP taken in different 100 mL quartz reactors. Prior to irradiation, the suspension was magnetically stirred in dark for 30 minute to establish the adsorption and desorption equilibrium. Then the suspension was exposed to solar light for 180 minutes in aerobic conditions. The average light intensity was around 10, 5000 Lx measured by using LT lutron Lx-101A digital light meter (nearly constant during the experiment). After irradiation, the suspension was centrifuged and the content of MG, RHG and CNP were analyzed quantitatively by using Varian Cary IE UV-vis spectrophotometer (model EL 96043181) at a wavelength corresponding to the maximum absorbance, 614 nm (MG), 547nm (RHG) and 280 nm (CNP).

The chemical oxygen demand (COD) is used to measure the oxygen equivalent of the organic content in the sample. So, this technique is based on the measurement of changes in oxygen concentration resulting in the photocatalytic oxidation of organic compounds and determined by standard conventional method using $K_2Cr_2O_7$.²⁵ The degradation of pollutants was followed by measuring the total organic carbon concentration using a TOC analyzer (ANATOC).

Analyses of hydroxyl radicals (OH[•])

The concentrations of the OH[•] generated from the LDHs during photocatalytic reaction were measured using a terephthalic acid (TA) fluorescence probe method. In this method, terephthalic acid readily reacts with [•]OH to produce a highly fluorescent product, 2-hydroxyl terephthalic acid, which shows the PL signal at 426 nm excited with 315 nm light. Experimental procedure was similar to the measurement of photocatalytic activity measurement except that 5×10^{-4} M terephthalic acid in 2×10^{-3} M NaOH solution was

used instead of dye solution. The PL spectra were measured on a Perkin-Elmer (LS 55) fluorescence spectrophotometer.

Superoxide radical detection.

For superoxide radical detection, electron paramagnetic resonance (EPR) spectra were recorded on a Bruker EMX X-band spectrometer with 100 kHz field modulation. The microwave frequency was calibrated using a frequency counter of the microwave bridge ER 041 XG-D. DPPH was used as a field marker ($g = 2.0036$). The irradiation light sources for EPR study are HPA 400/30S lamp (400 W, Philips). The magnetic field values of radicals were determined by employing the formula, $h\nu = g\beta H$.

RESULTS AND DISCUSSION

Structural, morphological and textural properties

The crystallographic structural characterizations of all the synthesized samples (ZB2, ZB3, ZB4, ZB_{H_y}4 and ZBV_{H_y}4) are investigated by PXRD (Fig.1). A single crystalline phase was formed in all the cases. All the reflection peaks ($00l$) could be indexed entirely to a brucite like structure with space group R-3m and hexagonal lattice. The presence of more amount of Bi³⁺ in the brucite layer during the co-precipitation process resulted in less ordered stacking of the brucite layers and lower crystallinity. As the ionic radius of Zn²⁺ (88pm) is lower than that of the ionic radius of Bi³⁺ (117pm), more amount of Bi³⁺ in the brucite layer results distorted the crystal lattice and pore crystallinity. Similar observation was noticed by us in case of Ce doped Zn-Al LDH.²⁶ Due to variation in molar proportion of Zn/Bi, the change in crystallographic properties of (110) plane is observed. The lattice parameter 'a' indicates the average cation to cation distance in the layers calculated based on the (110) peak position increases with the concentration of Bi³⁺ ions in the samples (Table S1). The sample (ZB_{H_y}4) prepared under hydrothermal conditions is more crystalline and phase pure possessing reflections at (003), (006), (009), and (110) plane with a basal spacing of 7.76 Å

[JCPDS: 41-1428]. These values coincide with those reported in the literature for carbonate-containing hydrotalcite materials.⁷⁻⁸ The exchange of carbonate/nitrate with decavanadate is illustrated (Scheme 1). In case of vanadate intercalated ZB_{Hy}4 LDH (ZBV_{Hy}4), the basal spacing value (d_{003}) is 11.9 Å along with other reflections recorded at 5.95 Å (14.9°) and 3.95 Å (22.4°) corresponding planes (006) and (009). As no peak is recorded close to 7.76 Å, it is presumed that carbonate species have been completely removed from the interlayer space of ZB_{Hy}V4 LDH. The exchange of interlayer anions $\text{CO}_3^{2-}/\text{NO}_3^-$ by $\text{V}_{10}\text{O}_{28}^{6-}$ depends on both pH and nature of the cations in the host structure.

According to reference,²⁷ the values of the lattice parameters, a and c , were calculated by means of the following equations and reported (Table 1);

$$a = 2d_{110}, c = 3d_{003}$$

The value calculated for parameter ' c ' is 35.7 Å for ZB_{Hy}V4 LDH, which is in agreement with the value reported by several authors for decavanadate-containing hydrotalcites.²⁸ There was almost no change in the d_{110} value after intercalation of the vanadate, indicating that the structure of the layers was retained. A considerable broadening of the peaks was observed in the case of ZBV_{Hy}4 LDH. Crystallite size is one of the important factors which played a significant role for the photocatalytic activity. To further highlight this effect, the average crystallite sizes of different samples were calculated by the Scherrer formula by using the (003) plane, which gave mean values for all the as prepared LDHs (Table 1).²⁹ Here the crystallite size of the samples followed the trend; ZB2 LDH > ZB3 LDH > ZB4 LDH > ZB_{Hy}4LDH > ZBV_{Hy}4 LDH.

The morphology of all LDHs was further systematically investigated by TEM analysis, as shown in Fig.2 (A, B and C). All the as prepared materials showed flake like particles. The selected area electron diffraction (SAED) pattern taken from these particles shown in the Fig.2 (D, E and F) clearly reveals the presence of concentric diffraction rings of

pure LDH phases and all are polycrystalline in nature. The crystallinity nature of ZB_{Hy}4 LDH and ZBV_{Hy}4 LDHs are higher than the ZB4 LDH, confirmed from our PXRD section. ZBV_{Hy}4 LDH did not give rise to any significant change in morphology.

To investigate the textural properties of LDH, the materials were analyzed by Brunauer–Emmett–Teller (BET) surface area by nitrogen adsorption-desorption measurement. To be a good candidate for a photocatalyst, its surface area is also important. N₂ adsorption–desorption isotherms of the samples are presented (in Fig. S2). The sorption isotherms of ZB_{Hy}4 is type III with H3 type hysteresis loop according to the BDDT classification and surface area is 71 m²/g. Hysteresis loop of H3 is always correlated with slit-shaped pores.³⁰ ZBV_{Hy}4 exhibits a typical IV isotherm with a H1-type hysteresis loop (P/P₀= 0.36) and surface area 140 m²/g, implying the presence of mesoporosity. Type H1 loops are often assigned to agglomerates or compact or spherical particles with uniform size.³¹ However, the surface area decreases with increasing Bi³⁺ content in the brucite layer reported in table 1 indicating low activity because the large surface area and the mesoporous materials are capable of allowing an easy diffusion of the pollutant molecules, resulting in higher photocatalytic activity.

The presence and nature of the charge-compensating anions of all LDHs were investigated by FTIR spectroscopy (illustrated in Fig.3). The broad absorption between 3600-3300 cm⁻¹ is due to stretching mode of hydrogen-bonded hydroxyl groups, both from the brucite-like layers and from the interlayer water molecules. The presence of a vibration band at 1360 cm⁻¹ is attributed to carbonate ions in case of ZB_{Hy}4. But the bands at 960, 815, 745, 598, and 505 cm⁻¹ are attributed to decavanadate species in the gallery.³² The band at 960 cm⁻¹ indicated the symmetric stretching mode of terminal V=O groups (ν_{v=0}), while the bands between 800 and 500 cm⁻¹ may be assigned to anti-symmetric and symmetric stretching modes of V-O-V chains. The band at 646 cm⁻¹ is assigned to the ν_{v-o}

in bridging V-O-V units in the tetrahedral chain. These results are in good agreement with the previous studies.³³

Optical properties

It is well-known that light absorption properties, generation and the migration of the light-induced charge carriers which are governed by the electronic structure and characteristics of a semiconducting material are the main key factors for controlling photocatalytic reactions.³⁴ The ZB_{H_y}4 LDH photocatalyst showed a broad absorption at about 420 nm assigned to overlapping of two bands, namely O²⁻ → Bi³⁺ ligand to metal charge transfer spectra (LMCT) for bismuth octahedron and another meant for metal-metal charge transfer spectra (MMCT) for Zn (II) –O–Bi (III) oxo-bridged system. In case of ZBV_{H_y}4 LDH, the absorption edge shifted towards visible region at about 530 nm (Fig. 4a). The results showed that the intercalated vanadate increases the absorbance of visible light and extends the absorption edge to longer wavelength because of the oxygen metal charge transfer spectra (OMCT) of O²⁻ → V^V in VO₆ octahedron. The absence of any band in the 600-800 nm range indicates the absence of V^{IV} species.³⁵

As discussed above, the visible light absorption by ZB_{H_y}4 is owing to MMCT excitation of the oxo-bridged Zn (II) –O–Bi (III) system. As, the oxo-bridged bimetallic linkages of LDHs are connected via two neighbouring octahedrons, and according to the oxidation state of Bi³⁺ cations in the bimetallic linkages of Zn-O-Bi LDH, the visible-light induced MMCT of Zn (II)-O-Bi (III) → Zn (I)-O-Bi (IV) is supposed to occur in this system. The excitation transition of an electron from one metal to other metal in oxo-bridged system with more than one type of metal differing in oxidation state is referred to as metal-to-metal charge transfer spectra. A lot of work has been documented on the visible-light induced MMCT for different oxo-bridged bimetallic systems.³⁶⁻³⁷ This is confirmed by the optical difference spectra following an exposure of the ZB_{H_y}4 LDH at 420 nm

irradiation for 6h in the presence of O₂ (inset Fig. 4(a)) where the absorption extends to visible range, clearly demonstrated. Red shift of the absorption is characteristic to MMCT since the absorption energy of MMCT is dominated by the difference in energy between the HOMO of acceptor and LUMO of donor elements.³⁸ Our recent work also revealed MMCT of the oxo-bridged bimetallic linkages of Zn (II)-O-Y (III) system.⁹

The band gap energy of both LDHs could be calculated by equation 1.

$$\alpha h\nu = A(h\nu - E_g)^{n/2} \quad (1)$$

Where α, ν, A and E_g are the absorption co-efficient, light frequency proportionality constant and band gap energy, respectively. In this case 'n' decided the characteristics of the transition of the materials i.e. direct transition or indirect transition. The method to evaluate the values of n has been reported elsewhere.³⁹ With use of this method, the value of n for both prepared LDHs were determined as 4 from their absorption spectra. This means that the optical transitions for both LDH materials are indirectly allowed. The band gap energy (E_g) can be estimated from the intercept of the tangents to the plots of $(\alpha (h\nu))^{0.5}$ against $h\nu$ photon energy as shown in Fig. 4(b). The band gap of ZBV_{H_y}4 was estimated to be 2.25 eV indicating narrow band gap as compared to ZB_{H_y}4 LDH (2.95).

Photoluminescence study

The photoluminescence (PL) emission spectra are useful to disclose the efficiency of charge carrier trapping, migration, transfer and separation of photogenerated electrons and holes in a semiconductor as it results from the recombination of free carriers; the lower PL intensity indicate lower recombination rate of the semiconductor.⁴⁰ In this study, the PL emission spectra of all LDH samples examined in the 400–600 nm is revealed (Fig. 5a). It is observed that a strong emission peak at approximately 470 nm is present in the spectra, associated with the radiative recombination of localized surface trapped charge carriers. The reduction in PL intensity indicates decrease in radiative recombination process.⁴¹ Likewise the other

small peaks about 500 nm may be due to the surface defect sites which showed green emission spectra and are also in agreement with the result of Wie's group.¹⁰⁻¹¹ Furthermore, the intensity of PL peak for ZB_{H_y}4 LDH is higher than the ZBV_{H_y}4 LDH. Therefore, it can be concluded that the recombination chance in case of ZB_{H_y}4 LDH is higher than that the ZBV_{H_y}4. The resultant depression of electron hole recombination is surely advantageous for the improvement in photocatalytic activity.⁴² So the intercalated vanadate can act as a charge trapping species retarding the electron hole recombination rate and improve the probability of photogenerated charge carrier separation and enhancing the photodegradation of organic pollutants.

Time-resolved photoluminescence spectroscopy was applied to study the dynamics of the photo generated carriers. In order to facilitate the reaction between photo-generated charges and organic contaminants, longer lifetime of photo generated charges is required. The emission decay data were analysed with bi-exponential kinetics in which decay components were derived.⁴³⁻⁴⁴ The life times (τ_1 and τ_2), pre-exponential factors (A1 and A2), and intensity-average life time ($\langle\tau\rangle$) for ZB4, ZB_{H_y}4 and ZBV_{H_y}4 LDH material were determined (Table 2) Typical fitting results to derive PL life times are shown (in Fig. 5 (b)). It can be clearly observed that the average lifetime of photo generated charges in ZBV_{H_y}4 LDH is 5.6 ns, which is 1.2 and 8 times longer than that of ZB_{H_y}4 LDH and ZB4 LDH, respectively. The long PL decay time for ZBV_{H_y}4 has been assigned to a low concentration of radiative defects in the materials. The longer lifetimes of photo generated charges are beneficial to react with target molecules.

Photo electrochemical measurement

In addition to optical response, we further investigated the photo electrochemical properties of the material by photocurrent measurement. The photocurrent plots of ZB_{H_y}4 and ZBV_{H_y}4 LDH are shown in (Fig.6 (a), (b)). The photo electrochemical measurement was carried out

at pH 6.5 vs. Ag/AgCl electrode in 0.1 M Na₂SO₄ solution. The result of photocurrent measurement for both the LDHs confirmed that the increase in photocurrent density with an increase in cathodic bias indicates the p-type conductivity of ZB_{Hy}4 and ZBV_{Hy}4 LDH, serving as photocathode.⁴⁵ Since both are p-type, the photocurrent onset potential for both cases provide the value of the valence band edge, from which the value of the conduction band edge is estimated. In the case of p-type semiconductor, photo-current is generated when the flat band potential exceeds applied potential.⁴⁶ The onset potential of ZB_{Hy}4 and ZBV_{Hy}4 LDH are determined by plotting I-V curves both in the dark and light illumination. The photocurrent onset potential (valence band edge) of both ZB_{Hy}4 and ZBV_{Hy}4 LDH were observed at +2.08 V and +2.15 V vs. Ag/AgCl at pH 6.5. As the HOMO – LUMO are no other than VB and CB respectively, the HOMO of ZB_{Hy}4 LDH and ZBV_{Hy}4 LDH was laying at +2.08 V and +2.15 V. Consequently, the position of LUMO energy levels for both ZB_{Hy}4 and ZBV_{Hy}4 LDH materials were at -0.87 V and -0.10 V vs. Ag/AgCl at pH 6.5. All these results indicate that the catalyst is a semiconductor strongly responsive to light irradiation. Under the same condition, ZBV_{Hy}4 LDH (+2.15 V) showed a higher oxidation ability (more positive valence band potential) than ZB_{Hy}4 LDH (+2.08 V) confirmed as a potential photo functional material and both are more positive than OH[•] / OH⁻ (~ +1.9 V), suggesting that both the as prepared LDHs could able to react with OH⁻/H₂O to form OH[•]. Therefore, the decomposition of dyes by LDHs could be due to the reaction with the photo generated OH[•] directly .

Photocatalytic activity

The photocatalytic performance of all the as prepared LDHs was investigated in terms of photodegradation of organic pollutants MG, RHG, and CNP under solar-light irradiation. Before monitoring the photocatalytic activity of the photocatalysts, simple photolysis and adsorption experiments were performed. It is observed that the characteristic spectra of the

pollutants in photolysis were remained unchanged even after 180 min. This confirms that the degradation of all pollutants is negligible or almost zero without adding any photo catalyst. Moreover, the experimental result predicts that MG, RHG and CNP in the aqueous solution are highly stable and inactive under visible light. Prior to solar light irradiation, the adsorption properties of all materials towards various dyes were examined in dark to establish the adsorption/desorption equilibrium. In dark conditions, about 20–25% organic pollutants are found to be adsorbed over these samples within 30 minutes, suggesting that there are no obvious differences among these samples in their abilities to adsorb MG, RHG and CNP in aqueous solution after 30 minutes and it could be seen that an equilibrium state of dye adsorption reached within 30 minute (figure S3). With the same initial concentration, low amounts of organic pollutants are adsorbed over all the as prepared LDHs. Under solar light irradiation, about ~ 90% of MG, 87% of RHG and 85% of CNP were degraded after 60 minutes by using ZBV_{H_y}4 LDH. However, after 180 minutes about ~ 65% and 45% of MG, 62% and 40% of RHG, 58% and 35% of CNP were decolorized by ZB_{H_y}4 LDH and ZB4 LDH, respectively, which confirmed ZB4 LDHs are less efficient than other LDHs under the same experimental conditions.

It has been widely reported that some degradation intermediates are more toxic and carcinogenic than the parent compounds. Hence, the complete mineralization of dye components prior to wastewater discharging is highly desirable.⁴⁷The TOC is a common water quality criterion, and its reduction is desirable. A complete disappearance of organic carbon would confirm the complete mineralization of pollutants. Fig.7 showed that the normalized TOC is in dependency with the irradiation time for all the organic pollutants. After 3 h of irradiation, the % of TOC removal from MG, RHG and CNP are about 80 %, 78 %, and 70 % over ZBV_{H_y}4 LDH, about ~75%, ~ 70% and 65% over ZB_{H_y}4 LDH and 40%, 32% and only 25% over ZB4 LDH, respectively. The result demonstrated that the

degradation process of all pollutants proceeds very rapidly over ZBV_{Hy}4 LDH. Also it may be noted that there is still some organic carbon was left out. So, complete degradation takes longer time than for the total disappearance of color of the pollutants in UV-Vis spectra.

The chemical oxygen demand (COD) is widely used as an effective technique to measure the organic strength of wastewater. The test allows measurement of waste in terms of the total quantity of oxygen required for oxidation of organic matter to CO₂ and water. The COD of all the solutions were estimated before and after the photo catalytic reaction using the K₂Cr₂O₇ oxidation method. The reduction in the COD values of the treated dye solution indicates the mineralization of dye molecules along with the color removal. Fig.8 gives the COD removal in mg/L and its efficiency after 180 minutes of light irradiation. The degradation efficiencies obtained after 180 minutes of irradiation were 91%, 78%, and 58% for MG, 85%, 78% and 55% for RHG, and 87% 75% and 52% for CNP over ZB4 LDH, ZB_{Hy}4 LDH and ZBV_{Hy}4, respectively, indicating that the rate of decolourisation of pollutants was noticeably faster in the case of ZBV_{Hy}4 than that of others.

To quantitatively understand the reaction kinetics of organic pollutants degradation, the Langmuir–Hinshelwood model was applied in photocatalytic experiments, as expressed by

$$-\frac{d[OP]}{dt} = k_{obs}[OP] \quad (2)$$

$$[OP] = [OP]_0, \quad \text{at } t=0 \quad (3)$$

$$\ln \frac{[OP]_0}{[OP]} = k_{obs}t \quad (4)$$

Also written as

$$\ln (C_0/C_t) = k_{obs}t \quad (5)$$

where ‘OP’ is organic products, k is the apparent reaction rate constant, C_0 is the concentration of aqueous pollutants at the reaction time t_0 , and C_t the concentration of the

pollutants at the reaction time t . Table S2 showed the values of k_{obs} and $t_{1/2}$ parameters (time required to degrade half of the initial concentration of dye). This result clearly indicates that the intercalated vanadate in ZB_{H_y}4 LDH required less than 18 minutes for degrading half of the initial concentration of all dyes.

To investigate the recyclability, the photocatalysts were collected after the photocatalytic reaction and reused in a photocatalytic reaction in successive three times under the same conditions. As shown in fig. S4, the as-synthesized catalyst displayed good stability and maintained a high photocatalytic performance during the three successive reaction cycles.

Discussion on possible photocatalytic mechanism

It is well known that the photocatalytic activity is mainly governed by crystal structure, adsorption ability, and separation efficiency of photo generated charge carriers.⁴⁸ It can be seen from the XRD spectra that ZB_{H_y}4 LDH exhibits more crystallinity than others. Garcia *et. el* found that the cation doping capacity at the octahedral sites of the brucite layers of the LDH act as a doped semi-conductor.⁶ Similarly, Bi³⁺ is substituted in the brucite layer of the LDHs and act as doped semi-conductors. Bi³⁺ has been found to be a more effective dopant for photocatalysis, this could promote the efficiency of electron-hole pair formation, separation and facilitate the transfer of excited electrons under visible light. Furthermore, this LDHs constituted the sheets of edge shared Bi {O (Zn)}₆ octahedral units where ZnO₆ edge shared octahedron links through BiO₆ octahedron to form three-dimensional tetrahedron. However, the ZnO₆ octahedron is active only in the UV-region, but the presence of Zn helps in getting better crystallinity. In BiO₆, it can be considered that the top of the VB is mainly composed of Bi 6s and O 2p, and the bottom of the CB is Bi 6s and Bi 6p. So, Bi 6s orbital have a large contribution towards top of the VB and the bottom of the CB.⁴⁹⁻⁵¹ According to HOMO and LUMO concept, HOMO - LUMO is no other than top of

the VB and bottom of the CB respectively. Additionally, a contribution from Bi 6s orbital was also observed for both the HOMO and LUMO and suggesting there is 's-to-s' excitation in the material. The photo generated electron transfer is also heavily affected by the orbital orientation. As 's' orbital has spherical symmetry, subsequently, s-s transition have lowest energy barriers and beneficial for the photo generated charge carriers. According to the previous result of density contour maps, the valence band maximum is considered as the Fermi level, and it is located at the A point in the first Brillouin zone, while the conduction band minimum is located at the V point.⁵² From the Touc plot and photocurrent measurement, it is observed that the transition is indirect and the system showed p-type character. This is in good agreement with the reported result.

The role of interlayer carbonate ion of LDHs towards the photocatalytic activity was less investigated, but recently our group¹⁴ demonstrates that the presence of carbonate in the interlayer inhibit the electron-hole recombination and significantly increases the photoactivity towards hydrogen evolution. By considering this point, we thought that carbonate intercalated ZB_{H_y}4 LDH under visible light irradiation would favor electron-hole separation and might be a cause for enhanced degradation of pollutants.

Investigation of active species

In the present study, the degradation rate of MG, RHG, and CNP over ZB4, ZB_{H_y}4 and ZBV_{H_y}4 LDHs showed a great decrease in the presence of benzoquinone (rate constant, $K = 6.1 \times 10^{-3} \text{ min}^{-1}$) and 2-Propanol (rate constant, $K = 1.0 \times 10^{-9} \text{ min}^{-1}$) {shown Fig. S5} which are scavengers of $\text{O}_2^{\cdot -}$ or $\cdot\text{OH}$, respectively. This clearly demonstrates the involvement of ROS in pollutant degradation.⁴³⁻⁵⁴

Detection of hydroxyl radicals and super oxide radicals

Moreover, to detect the presence of OH^{\cdot} radicals, we used terephthalic acid (TA) as a fluorescent probe. A gradual increase in PL intensity at about 426 nm is observed with time

for all materials. However, no PL intensity increase is observed in the absence of visible-light irradiation. This suggests that the fluorescence is from the chemical reaction between terephthalic acid and $\cdot\text{OH}$ formed during photocatalytic reactions. TA reacts with $\text{OH}\cdot$ readily to produce a highly fluorescent product, 2-Hydroxy terephthalic acid whose PL intensity is proportional to the amount of hydroxyl radicals.¹⁴ Fig.9 demonstrated the comparison of PL intensity for different samples at 30 min. It can be easily seen that the amount of $\text{OH}\cdot$ radicals produced by $\text{ZBV}_{\text{Hy}4}$ is larger than that of other catalysts. According to the reported result, the photo generated holes on the surface of bismuth-containing photocatalysts cannot react with H_2O to form $\text{OH}\cdot$ under visible light due to the low standard redox potential of $\text{Bi}^{4+}/\text{Bi}^{3+}$ ($E^0 = 1.59$), compared to $\text{HO}_2/\text{OH}\cdot$ (1.99 V).⁵⁰ But according to our PEC result, the higher oxidation ability (more positive valence band potential) of $\text{ZBV}_{\text{Hy}4}$ LDH and $\text{ZB}_{\text{Hy}4}$ LDH could be able to form $\text{OH}\cdot$. Also, the surface $\text{OH}\cdot$ groups of the LDHs are capable to form $\text{OH}\cdot$ radical which play an important role in the photocatalytic reaction. Thus, it is confirmed that hydroxyl radicals are active species and indeed participate in photocatalytic reactions. The photocatalysis is basically a surface phenomenon that is being very sensitive to the amount of surface OH groups which may act as the principal reactive oxidant in the photo reactions.

Furthermore, the identification of $\text{O}_2^{\cdot-}$ radicals was studied by EPR (Fig. 10). $\text{ZB}_{\text{Hy}4}$ LDH was subjected to a thermal treatment in vacuum at 473 K, followed by exposure to oxygen environment at room temperature prior to EPR measurement. As observed, the EPR spectrum of materials measured with O_2 under visible irradiation ($\lambda > 400$ nm) shows a signals at $g_z = 2.003$, $g_y = 2.011$, $g_x = 2.0037$ coincide to the g-tensor of the superoxide radicals,⁵⁵ which is formed by the interaction of Bi (III) with the adsorbed O_2 to form $\{\text{Bi (III)} + \text{O}_2 \rightarrow \text{Bi (IV)} + \text{O}_2^{\cdot-}\}$. Therefore the excitation of $\{\text{Bi (III)} + \text{Zn (II)} \rightarrow \text{Bi (IV)} + \text{Zn (I)}\}$ act as a new class of visible-light-sensitive redox centers which are responsible for the

degradation of dyes. During this process, the generated Zn (I) can be trapped by the adsorbed O₂ molecules and return to Zn (II), producing the superoxide radicals and also Bi (IV) reduced to Bi (III) by extracting one electron from the oxidizing dye molecules. In such a recycle process of electron transfer, the superoxide anion radical could be generated continuously. Ultimately, Bi (III) species are not consumed in the reaction. Here the Bi³⁺ of s² ions behaved as electron-donating ions to M(d¹⁰) ions, so there is usually a low-lying MMCT state which has been reported by others.⁵⁶ During visible-light irradiation, the heightening of EPR intensity of ZB_{H_y}4LDH than ZB4LDH suggest the formation of more number of superoxide radicals. But the intensity of ZB_{H_y}4 LDH and ZBV_{H_y}4 LDH are remained identical. Consequently, we believe that for both the cases, the Bi (III) species which have metal-oxygen-metal sites can originate visible-light induced MMCT transition upon visible-light irradiation. So, the ability of the oxo-bridged linkage act as a visible-light induced redox center to drive a photoreaction was demonstrated by the degradation of pollutants in aqueous solution upon visible-light irradiation. It is proposed that the local coordination environment of octahedron units (metal-oxygen-metal bond) in ZB_{H_y}4 LDH would have a significant influence on the photocatalytic activity.

Enhancement in photocatalytic activity of ZBV_{H_y}4 LDH

However, in vanadate intercalated LDH, some additional factors may be contributing for the improvement of photocatalytic activity. Decavanadate are made of octahedral packed 10 edge-sharing [VO₆] octahedron where V⁵⁺ ions polarized bonded with terminal O²⁻ ligands resulting in closed clusters with D_{2h} symmetry. The structure, which is based on a sodium-chloride-like arrangement of V and O atoms, has a close relationship to other isopoly complex molybdates, niobates, and tantalates. So the DRS spectra are characterized by charge-transfer (CT) transitions of the type O → V⁵⁺ and d-d transitions of V⁵⁺, and their energies are dependent on the oxidation state and coordination environment.⁵³ The distorted

VO₆ octahedron was essential for the photocatalysis due to large dipole moment in the materials, which could facilitate the electron hole separation. In the case of photocatalytic reaction over vanadate intercalated LDH, both are responsible i.e. BiO₆ and also interlayer vanadate. From the molecular orbital energy level diagrams, predicted on the basis of group theoretical analysis for vanadate bearing T_d symmetry, it can be seen that the HOMO is nonbonding fully filled oxygen 2p orbital with t₁ symmetry and that the LUMO is the molecular orbital contributing V(3d orbital) with symmetry 'e'.⁵⁷ Thus, the mode of activation of the catalyst is photonic activation by exciting the catalyst by absorbing high energy than the band gap energy which leads an intermolecular O_{2p} → V(3d) charge transfer spectra assigned as HOMO → LUMO Oxygen metal charge transfer spectra (OMCT).

By using semiconductor notation, the excitation of ZBV_{Hy}4 at the OMCT band can be presented as follows:



Therefore, we can suppose that photo generated OH* and O₂^{·-} radicals are responsible for photocatalytic degradation pathway of organic pollutants.

CONCLUSIONS

In summary, the photocatalytic activity evaluation, via the photo-degradation of various color and colorless pollutants under solar light demonstrated that ZB_{Hy}4 LDH exhibited much higher photocatalytic activity than ZB4 LDH. The enhanced photocatalytic activity of ZB_{Hy}4 LDH is attributed to (i) High crystallinity and phase purity (ii) 's-to-s' excitation of BiO₆ octahedron (iii) low recombination of charge carriers confirmed by PL (iv) act as a oxo-bridged system possessing a number of metal-oxygen-metal sites that are able to

produce superoxide radicals and (v) long photogenerated charge lifetime. The intercalating of vanadate in the interlayer of $ZB_{Hy}4$ LDH ($ZBV_{Hy}4$ LDH) gives promising result in terms of degradation time and mineralization compared to other LDHs. The superior performance in short time period of $ZBV_{Hy}4$ could be attributed to its lowest crystallite size, high surface area, and higher oxidation ability (more positive valence band potential calculated from PEC study). The long-lived exciton and broad visible absorption could potentially furnish materials for photocatalysis. Furthermore, the presence of distorted VO_6 octahedron of decavanadate was essential for the photocatalysis due to large dipole moment in the materials, which could facilitate the electron hole separation confirmed by PL. It is suggested that the vanadate intercalated bismuth doped LDH can promote the transfer of the excited carriers and prolong the life time of the carriers on the surface leading to the enhancement of the activity for photocatalytic reaction.

Acknowledgments

The authors are thankful to Dr. D. Srinivas, NCL, Pune, India for EPR study. Lagnamayee Mohapatra is extremely grateful to CSIR New Delhi for awarding her SRF.

REFERENCES

- 1 W. Shi, Y. Lin, S.Zhang, R.Tian, R. Liang, M.Weil, D.G.Evans, X.Duan, *Phys.Chem.Chem.Phys.*, 2013, **15**,18217.
- 2 K.Jayanthi, and P. V. Kamath, *Dalton Trans.*, 2013, **42**, 13220.
- 3 X. D. B. Vos, M. Buntinx, K.D. Pierard, A. Mesmaeker, P. Jacobs, *Nature*, 1999, **400**, 855.
- 4 Z. Liu, R. Ma, M. Osada, N. Iyi, Y. Ebina, K. Takada, T. Sasaki, *J. Am. Chem. Soc.* 2006, **128**, 4872.
- 5 Y.Zhang, B. Cui, C. Zhao, H. Lin, J. Li, *Phys.Chem.Chem.Phys.*, 2013, **15**,7363.

- 6 C. Silva, Y. Bouizi, V. Fornes, H. Garcia, *J. Am. Chem. Soc.* 2009, **131**,13833.
- 7 K. M Parida, L. Mohapatra, *Dalton Trans.* 2012, **41**, 1173.
- 8 K. M. Parida, L. Mohapatra, *Chem. Eng. J.* 2012, **179**, 131.
- 9 K. M. Parida, L. Mohapatra, M. Satpathy, *J. Phys. Chem. C*, 2012, **116**, 13063.
- 10 Y. Zhao, S. Zhang, B. Li, H. Yan, S. He, L. Tian, W. Shi, J. Ma, M. Wei, D. G. Evans, *Chem. Eur. J.* 2011, **17**, 13175.
- 11 Y. Zhao, P. Chen, B. Zhang, D. S. Su, S. Zhang, L. Tian, J. Lu, Z. Li, X. Cao, B. Wang, M. Wei, D. G. Evans, X. Duan, *Chem. Eur. J.*, 2012, **18**,11949.
- 12 L. Mohapatra, K. M. Parida, N. Baliarsingh, *J. Phys. Chem. C*, 2012, **116**, 42417.
- 13 K. M. Parida, M. Satpathy, L. Mohapatra, *J. Mater. Chem.* , 2012, **22**, 7350.
- 14 N. Baliarsingh, L. Mohapatra, K. M. Parida, *J. Mater. Chem. A* 2013, **1**, 4236.
- 15 Lee, Y. ; Choi, J. H. ; Jeon, H. J. ; Choi, K. M. ; Lee, J. W. ; Kang, J. K. *Energy Environ. Sci.*, 2013, **6**,1008.
- 16 E. Geraud, S. Rafqah, M. C. Sarakha, V. P. Forano, F. Leroux, *Chem. Mater.*, 2008, **20**,1116.
- 17 S. Tokunaga, H. Kato, A. Kudo, *Chem.Mater.*, 2001, **13**, 4624.
- 18 J. Yu, Kudo, A. *Adv. Funct. Mater.* 2006, **16**, 2163.
- 19 S. Kohtani, M. Koshiko, A. Kudo, K. Tokumura, Y. Ishigaki, A. Toriba, K.;Hayakawa, R. Nakagaki, *Appl.Catal.B*, 2003, **46**, 573.
- 20 J. Tang, Z. Zou, J. Ye, *Catal.Lett.*, 2004, **92**, 1.
- 21 H. Fu, L. Zhang, W. Yao, Y. Zhu, *Appl.Catal.B*, 2006, **66**,100.
- 22 C. Zhang, Zhu, Y. *Chem.Mater.* 2005, **17**, 3537.
- 23 J. Luo, P.A. Maggard, *Ad .Mater.*, 2006, **18**,514.
- 24 F. Kooli, M. A. V.Rives, Ulibarri, *Inorg. Chem.* 1995, **34**, 5122.

- 25 ALPHA, Standard Methods for the Examination of Water and Wastewater, 20th ed.; American Public Health Association: Washington, DC, 1998.
- 26 J. Das, D. Das, K.M. Parida, *J. Colloid Interface Sci.* 2006,**301**,569.
- 27 U. Costantino, M. Casciola, L. M. linelli, *Solid state Ionics*, 1997, **97**, 203.
- 28 F. Kooli, W. Jones, *Inorg. Chem.*1995, **34**, 6237.
- 29 KamalK.Gupta,A.Kundan,P. K.Mishra,P. Srivastava,S.Mohanty,N. K.Singh,A. Mishrad P.Maiti, *Phys.Chem.Chem.Phys.*, 2012, **14**,12844.
- 30 C. J. Lia, G. R. Xua, B. Zhanga, J. R. Gong, *Applied Catalysis B:Environmental* ,2012,**115**, 201.
- 31 C. A. Castro, A. Jurado, D. Sissa, S. A. Giraldo, *Int. J.of Photoenergy*, 2011, **2012**, 1.
- 32 E. L. Salinas, Y. Ono, *Bull.Chem. SOC. Jpn.*, 1992, **65**, 2465.
- 33 J. Fuchs, S. Mahjour, R. Z. Palm, *Naturforsch*, 1976, **31**, 537.
- 34 L. D. Frederickson Jr, D. M. Hansen, *Anal. Chem.*, 1978, **23**, 93.
- 35 S. Sun, W. Xu, H. Wang, L. Zhou, M. Shang, L. Zhang, *J. Phys. Chem. C*, 2008, **112**, 17835.
- 36 Z.Li, Y.Dai, X.Ma,Y.Zhu,B.Huang *Phys.Chem.Chem.Phys.*2014,**16**,3267.
- 37 W. Lin, H. Frei, *J. Phys.Chem B.*, 2005, 109, 4929.
- 38 R. Nakamura, A. Okamoto, H. Osawa, H. Irie, K. Hashimoto, *J. Am. Chem. Soc.* **2007**, 129, 9596.
- 39 W. P. Griffith, P.J. B. Lesniak, *J. Chem. Soc. A*, 1969, **1066**.
- 40 Y.Cong, J. Zhang, F.Chen, M. Anpo, D. He, *J.Phys.Chem.C* **2007**, 111, 10618 .
- 41 H. Tang, K. Prasad, R.Sanjines, P.E.Schmidd, F. Levy, *J.Appl.Phys.* **1994**, 75,2042.
- 42 S.Sajjad,S. A.K. Leghari, F. Chen, J. Zhang, *Chem.Eur.J.* 2010, 16,13795.
- 43 T. T. Yang, Chen, W. T.; Hsu, Y. J.; Wei, K. H.; Lin, T. Y.; Lin, T.W. *J. Phys. Chem.C* **2010**,114, 11414.

- 44 X. Chen, Y.S. Jun, K. Takanahe, K. Maeda, K. Domen, X. Fu, Antonietti, M.; Wang, X. *Chem. Mater.*, 2009, **21**, 4093.
- 45 A. L. Linsebigler, G. Lu, J. T. J. Yates, *Chem. Rev.*, 1995, **95**, 735.
- 46 D.W. Hwang, J. Kim, T. J. Park, J. S. Lee, *Catal. lett.*, 2002, **80**,1.
- 47 C. Jakopitsch, G. Regelsberger, P. G. Furtmuller, F. Ruker, G. A. Peschek, C. Obinger, *Biochem. Biophys. Res. Commun.*, **2001**, 287,682.
- 48 X. Xiao, C. Liu, R. Hu, X. Zuo, J. Nan, L. Li, L. Wang, *J. Mater. Chem.*, 2012, **22**, 22840.
- 49 J. Tang, Zou, Z.; Ye, J. *J. Phys. Chem. C*, 2007, **111**, 12779.
- 50 D.A. Papaconstantopoulos, *Phys. Re .B*, 1989, **40**, 8844.
- 51 L.F. Mattheiss, D.R. Hamann, *Phys.Re.B*, 1983, **28**,4227.
- 52 J. Tang, Z. Zou, J. Ye, *J. Phys. Chem. C*, 2007,**111**, 12779.
- 53 M. Juan, A. Coronado, J. Maira, J. C. Conesa, K. L. Yeung, V. Augugliaro, J. Soria, *Langmuir*, 2001, **17**, 5368.
- 54 L. Zhang, Y. Zhu, *Catal. Sci. Technol.*, 2012, **2**,694.
- 55 Lin, W.; Frei, H. *J.Am.Chem.Soc.*, 2005,**127**,1610.
- 56 G. Blasse, *Structure and Bonding*, Springer-Verlag Berlin Heidelberg, 1991.
- 57 J. T. E Howard, *Inorg. Chem.*, 1966, **5**, 967.

Table captions

Table 1. Cell parameters, Average Crystallite size, BET Surface area of all as prepared LDHs.

Table 2. Photogenerated charge lifetimes of all as prepared materials.

Scheme captions

Scheme 1. Schematic representation of nitrate/carbonate exchange with decavanadate in layered double hydroxide; d spacing were calculated from XRD analysis.

Figure captions

Fig. 1 PXRD pattern of all the samples (Inset: PXRD pattern of ZB2, ZB3, and ZB4)

Fig. 2 TEM image of (a) ZB4LDH (b) ZB_{Hy}4 LDH (c) ZBV_{Hy} 4 LDH and SAED pattern of (d) ZB4LDH (e) ZB_{Hy}4 LDH (f) ZBV_{Hy} 4 LDH.

Fig. 3 FTIR spectra of ZB_{Hy}4 LDH and ZBV_{Hy} 4 LDH.

Fig. 4 (a) UV–Vis diffuse reflectance spectra of ZB_{Hy}4 LDH and ZBV_{Hy} 4 LDH (Inset: UV vis diffuse reflectance spectra of ZB_{Hy}4 before and after exposure to 420 nm irradiation for 6h in the presence of O₂) (b) Band gap energy of ZB_{Hy}4 LDH and ZBV_{Hy} 4 LDH.

Fig. 5 Fluorescence spectra of all the as prepared LDHs (a) ZB4LDH (b) ZB_{Hy}4 LDH (c) ZBV_{Hy} 4 LDH.

Fig. 6 Current–potential curves for (a) ZB_{Hy}4 LDH and (b) ZBV_{Hy} 4 LDH under dark and light irradiation in 0.1 M Na₂SO₄ aqueous solutions at pH 6.5.

Fig. 7 % of TOC removal over (a) ZB4LDH (b) ZB_{Hy}4 LDH (c) ZBV_{Hy} 4 LDH. .

Fig. 8 Photocatalytic degradation of all pollutants (a) MG (b) RHG (c) CNP with all prepared LDHs by COD (mg/L) and photodegradation efficiency (%).

Fig. 9 PL spectral changes with visible-light irradiation time over all as prepared samples in a 5×10^{-4} M basic solution of terephthalic acid.

Fig. 10 EPR spectra of (a) ZB4LDH (b) ZB_{Hy}4 LDH (c) ZBV_{Hy}4 LDH.

Supporting Information

Fig. S1 The structures of (a) Malachite green (b) Rhodamine 6G (c) 2 nitro-4-chloro phenol.

Fig. S2 The nitrogen sorption isotherm of all as prepared LDHs.

Fig. S3 Adsorption, Photolysis and photocatalytic degradation of (a) MG (b) RHG (c) CNP in aqueous solution (80 ppm) with all as prepared LDHs.

Fig. S4 Recycle test of the (a) ZB_{Hy}4 LDH and (b) ZBV_{Hy}4 LDH.

Fig. S5 Photocatalytic degradation of MG, RHG, and CNP for as prepared LDHs under visible irradiation in the presence of different quencher.

Table S1 The values of k_{obs} and $t_{1/2}$ parameters (time required to degrade half of the initial concentration of dyes).

Table 1. Cell parameters, Average Crystallite size, BET Surface area of all as prepared LDHs.

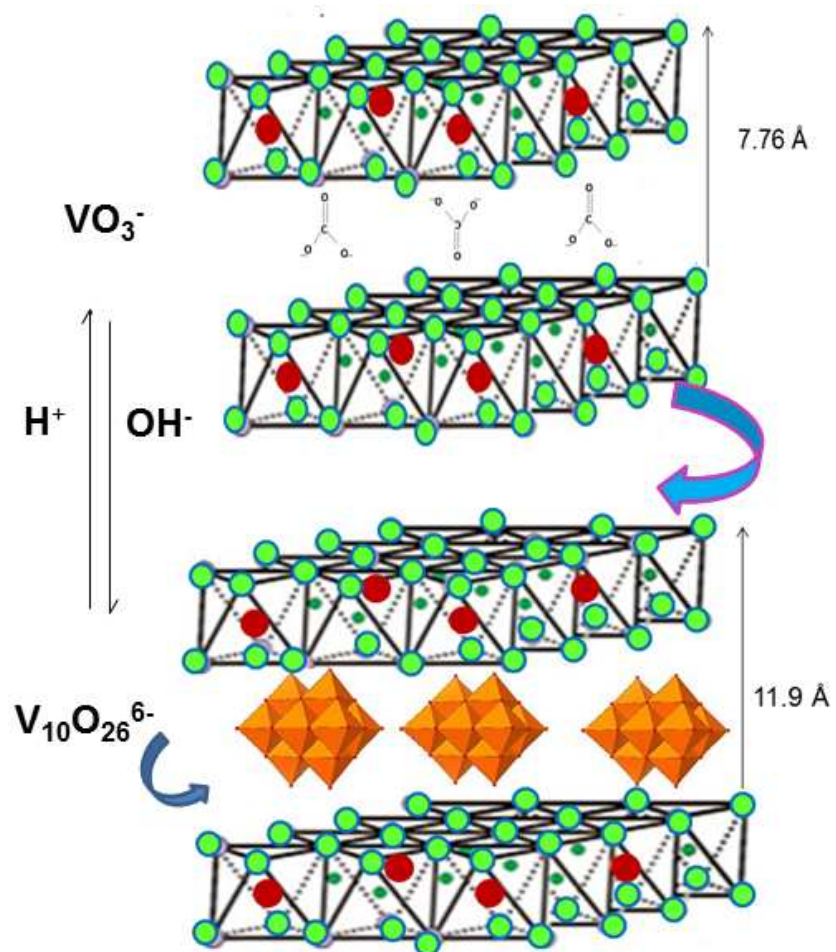
All Datas in the table1 were calculated from the XRD.

Catalysts	Structural parameter (Å)			Average Crystallite size	BET Surface area
	d_{003}	'c'	'a'	(Å)	m^2/g
ZB2 LDH	7.76	23.3	3.09	36	35
ZB3 LDH	7.76	23.3	3.07	33	54
ZB4 LDH	7.76	23.3	3.06	30	58
ZB 4 LDH	7.76	23.3	3.06	29	69
ZB _{Hy} 4 LDH	7.76	23.8	3.06	17	71
ZBV _{Hy} 4 LDH	11.9	35.7	3.06	11	140

Table 2. Photogenerated charge lifetimes of all as prepared materials.

All Datas in the table 2 were calculated from the Time-resolved photoluminescence (PL) spectra.

Sample	a1	τ 1	a2	τ 2	τ
ZB 4 LDH	7278.9	6.1389	3049.4	4.023	0.70
ZB _{Hy} 4 LDH	5594	2.2482	4395.1	5.7204	4.5
ZBV _{Hy} 4 LDH	6013.9	6.3234	4687.9	4.1966	5.6



Scheme 1. Schematic representation of nitrate/carbonate exchange with decavanadate in layered double hydroxide; d spacing were calculated from XRD analysis.

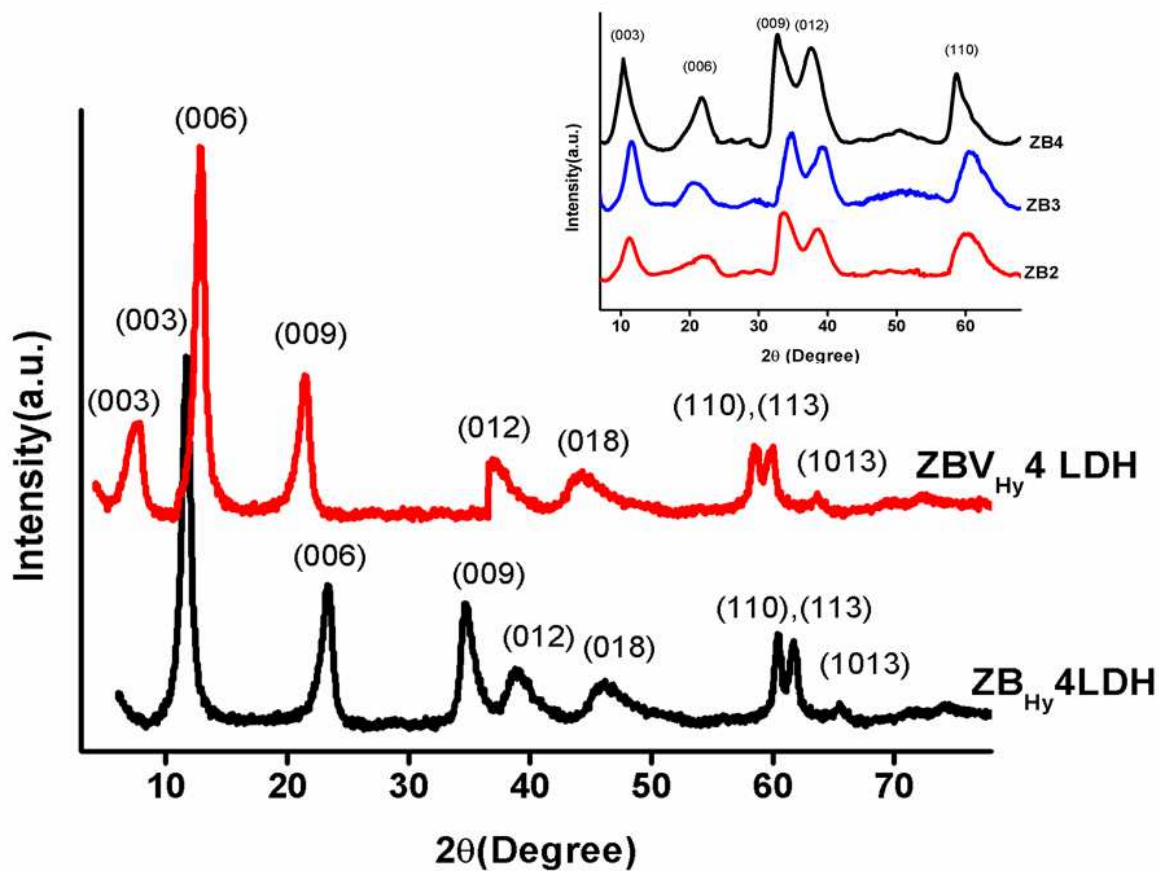


Fig. PXRD pattern of all the samples (Inset: PXRD pattern of ZB2, ZB3, and ZB4)

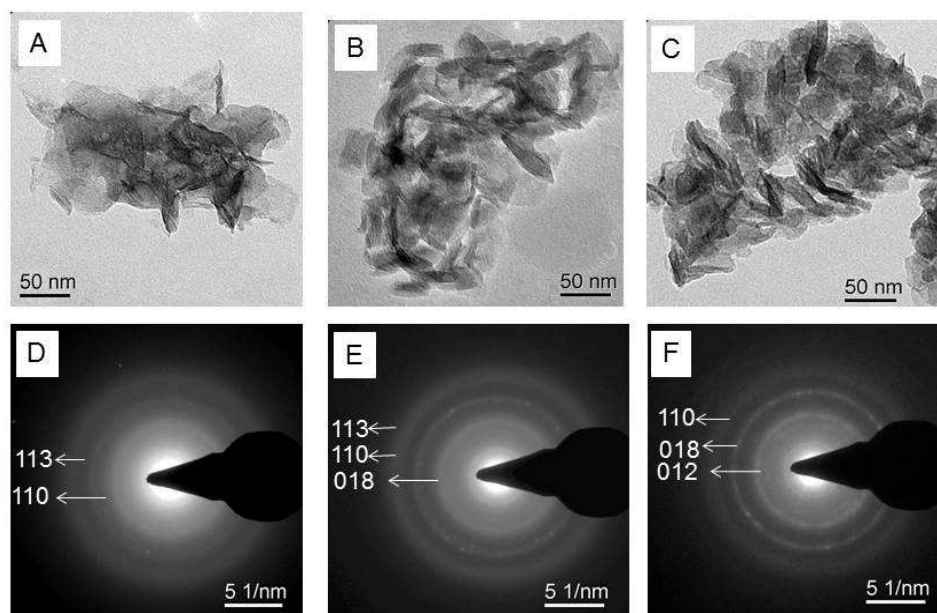


Fig. 2 TEM image of (a) ZB₄ LDH (b) ZB_{H_y}₄ LDH and (c) ZBV_{H_y}₄ LDH and SAED pattern of (d) ZB₄ LDH (e) ZB_{H_y}₄ LDH and (f) ZBV_{H_y}₄ LDH.

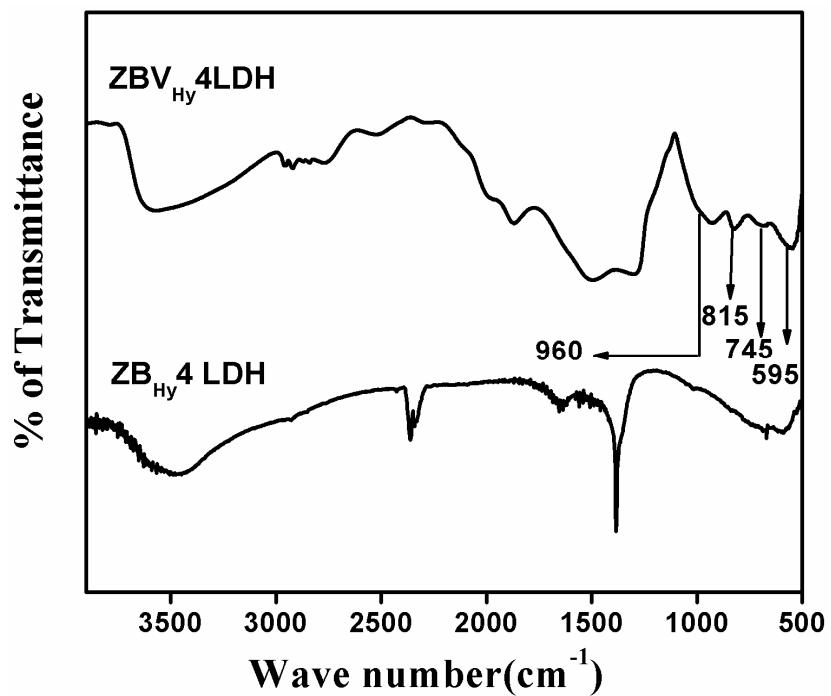


Fig. 3 FTIR spectra of $ZB_{Hy}4LDH$ and $ZBV_{Hy}4LDH$

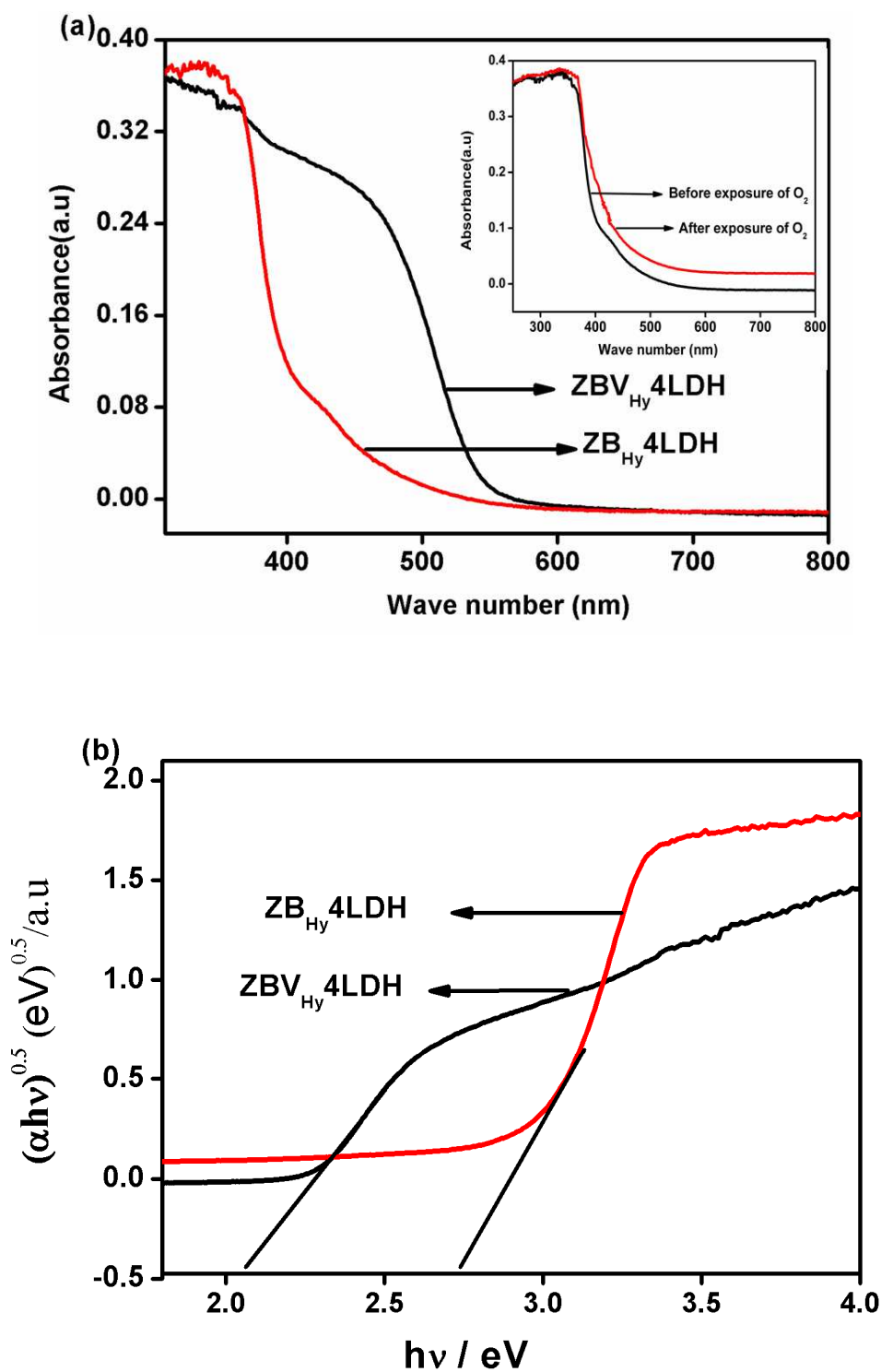


Fig. 4 (a) UV-Vis diffuse reflectance spectra of $ZB_{Hy}4$ and $ZBV_{Hy}4$ LDH (Inset: UV-Vis diffuse reflectance spectra of $ZB_{Hy}4$ LDH before and after exposure to 420 nm irradiation for 6h in the presence of O_2) (b) Band gap energy of $ZB_{Hy}4$ and $ZBV_{Hy}4$ LDH.

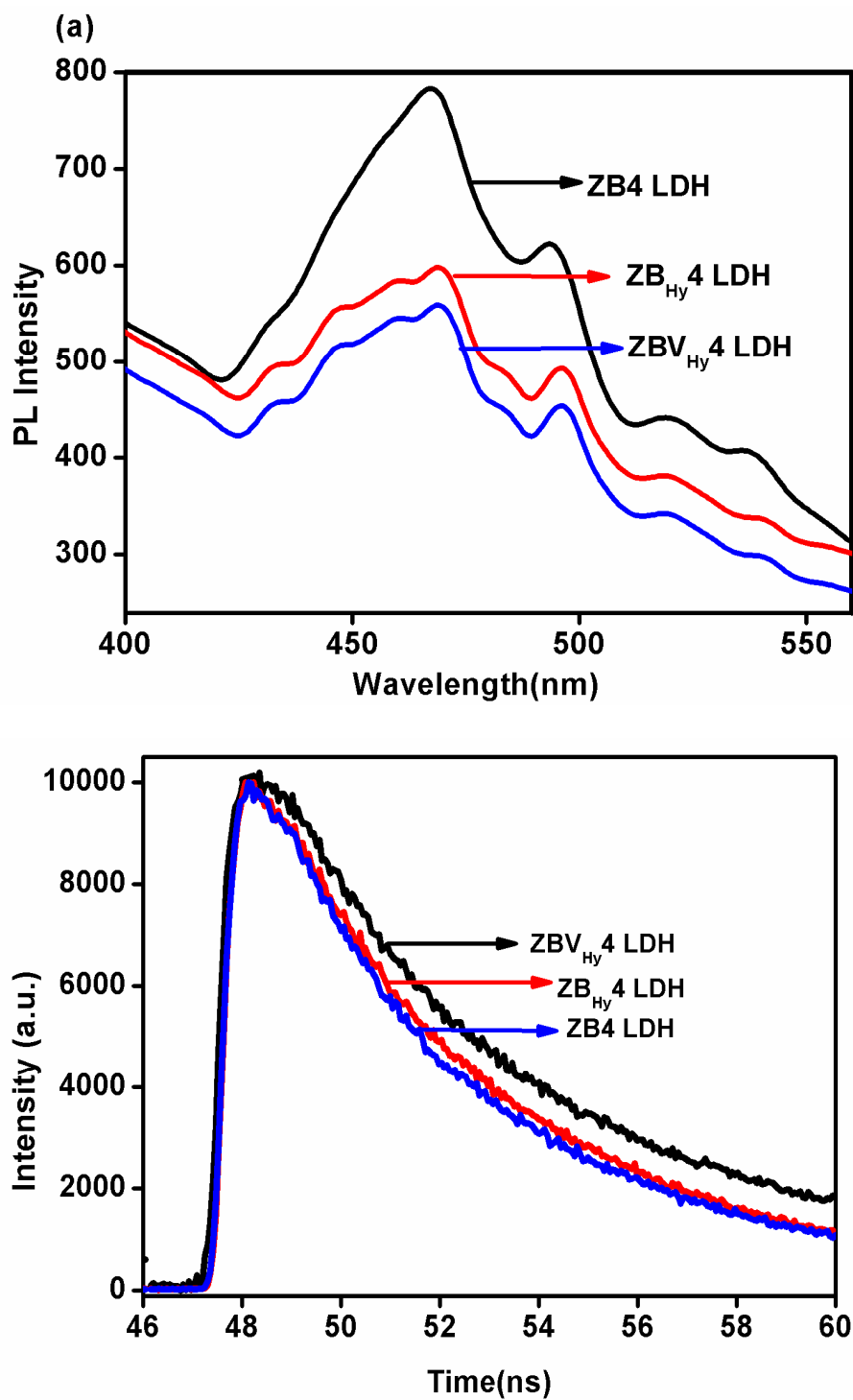


Fig. 5 (a) Fluorescence spectra and (b) Time-resolved PL-spectra of ZB4LDH, ZB_{Hy}4 LDH and ZBV_{Hy}4 LDH.

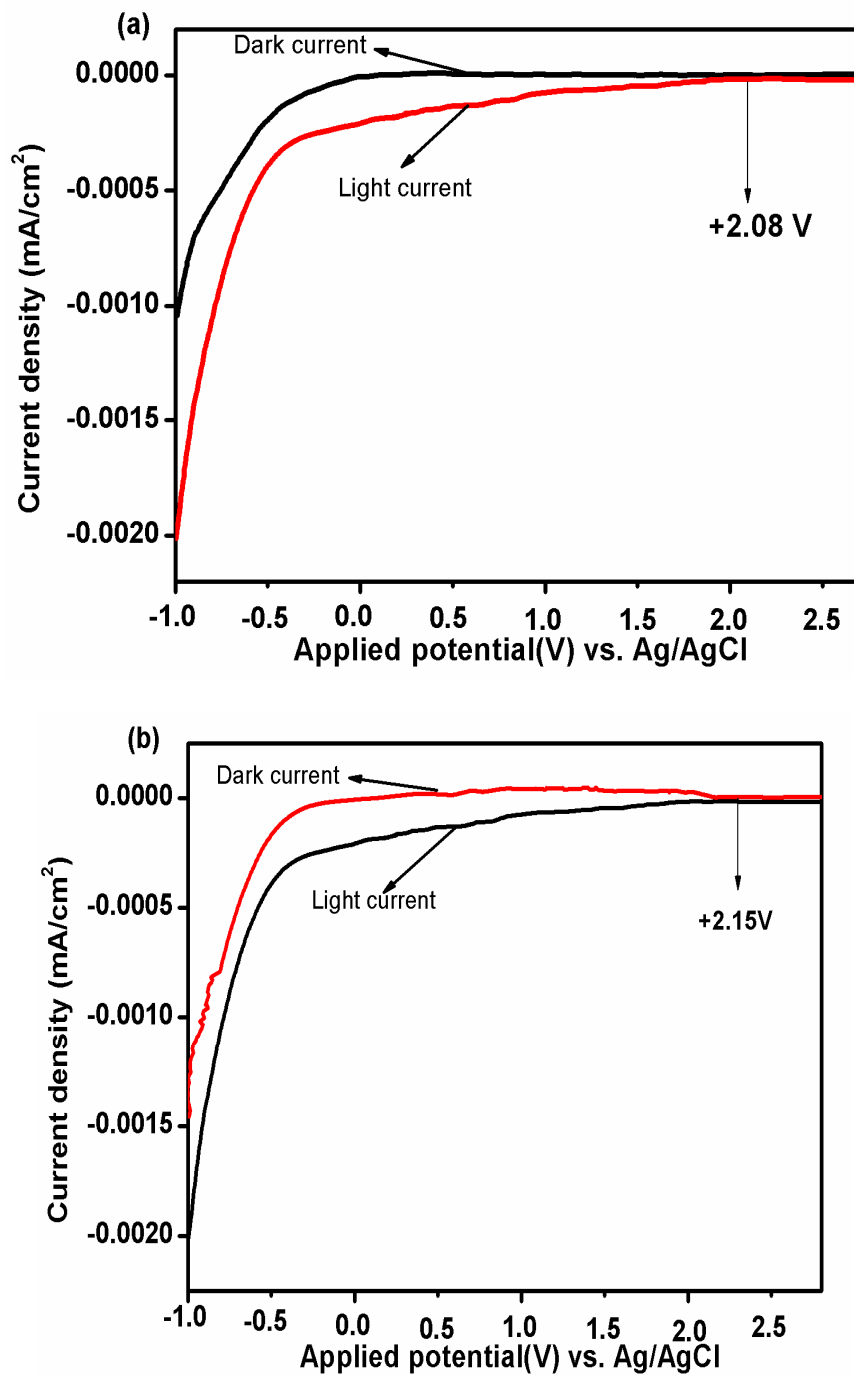


Fig. 6 Current–potential curves for (a) ZB_{Hy}4 LDH and (b) ZBV_{Hy}4 LDH under light irradiation in 0.1 M Na₂SO₄ aqueous solutions at pH 6.5.

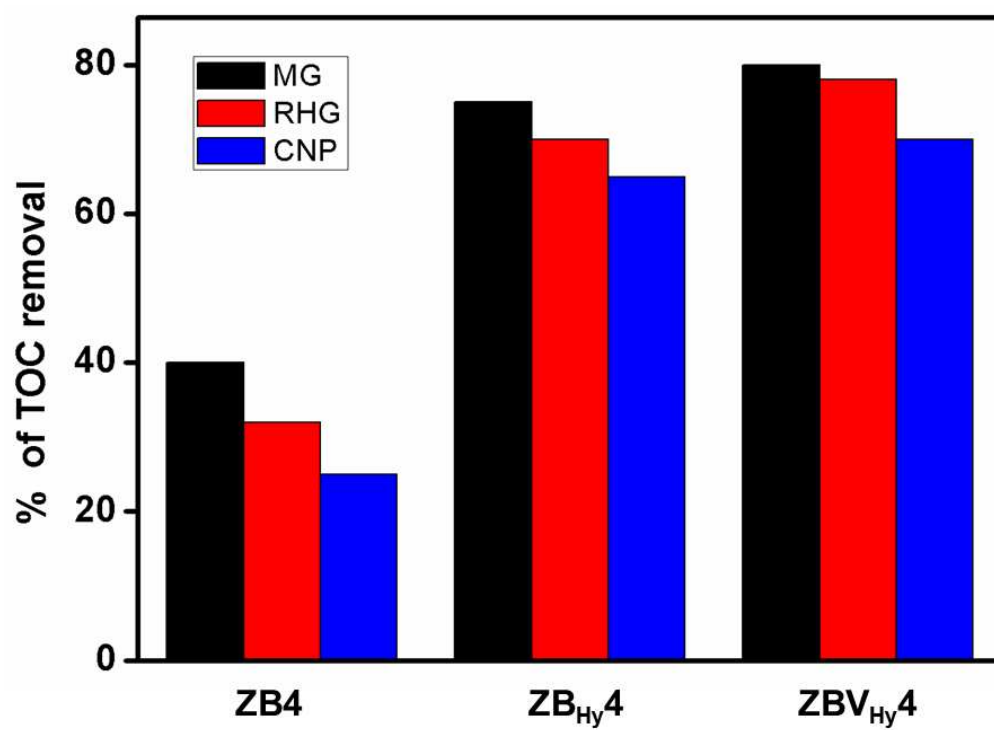
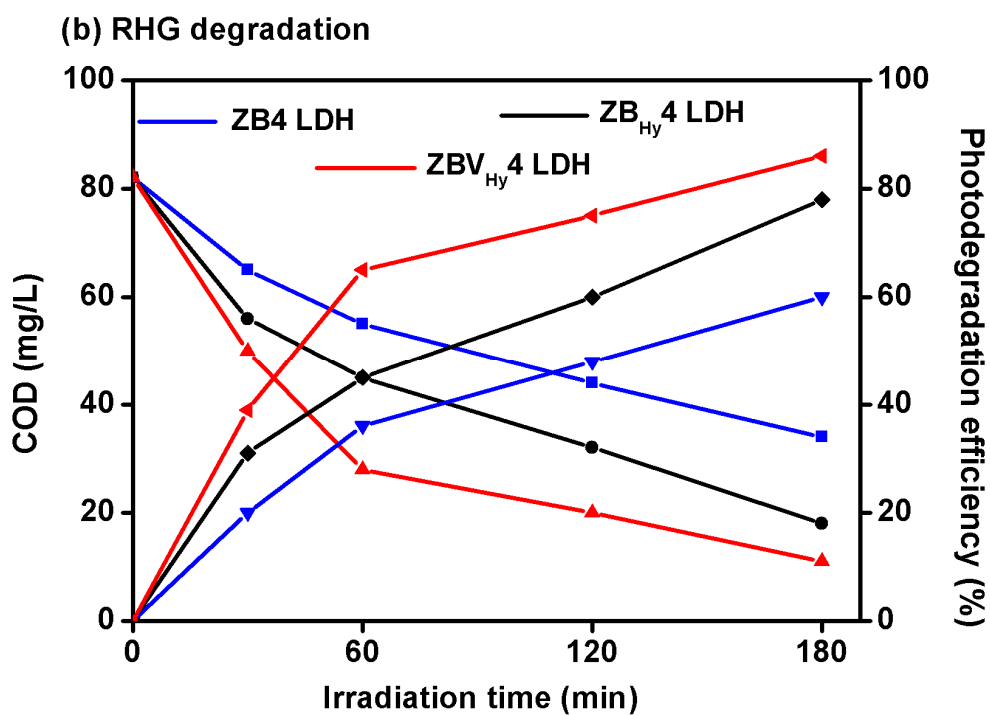
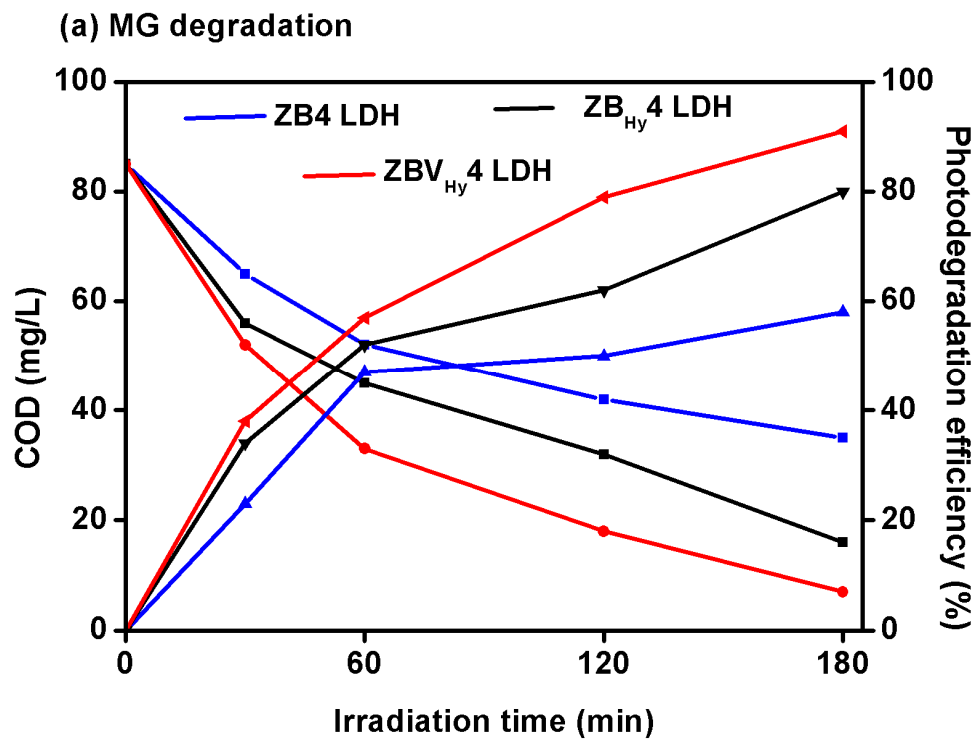


Fig. 7 % of TOC removal over ZB4LDH, ZB_{Hy}4 LDH and ZBV_{Hy}4 LDH.



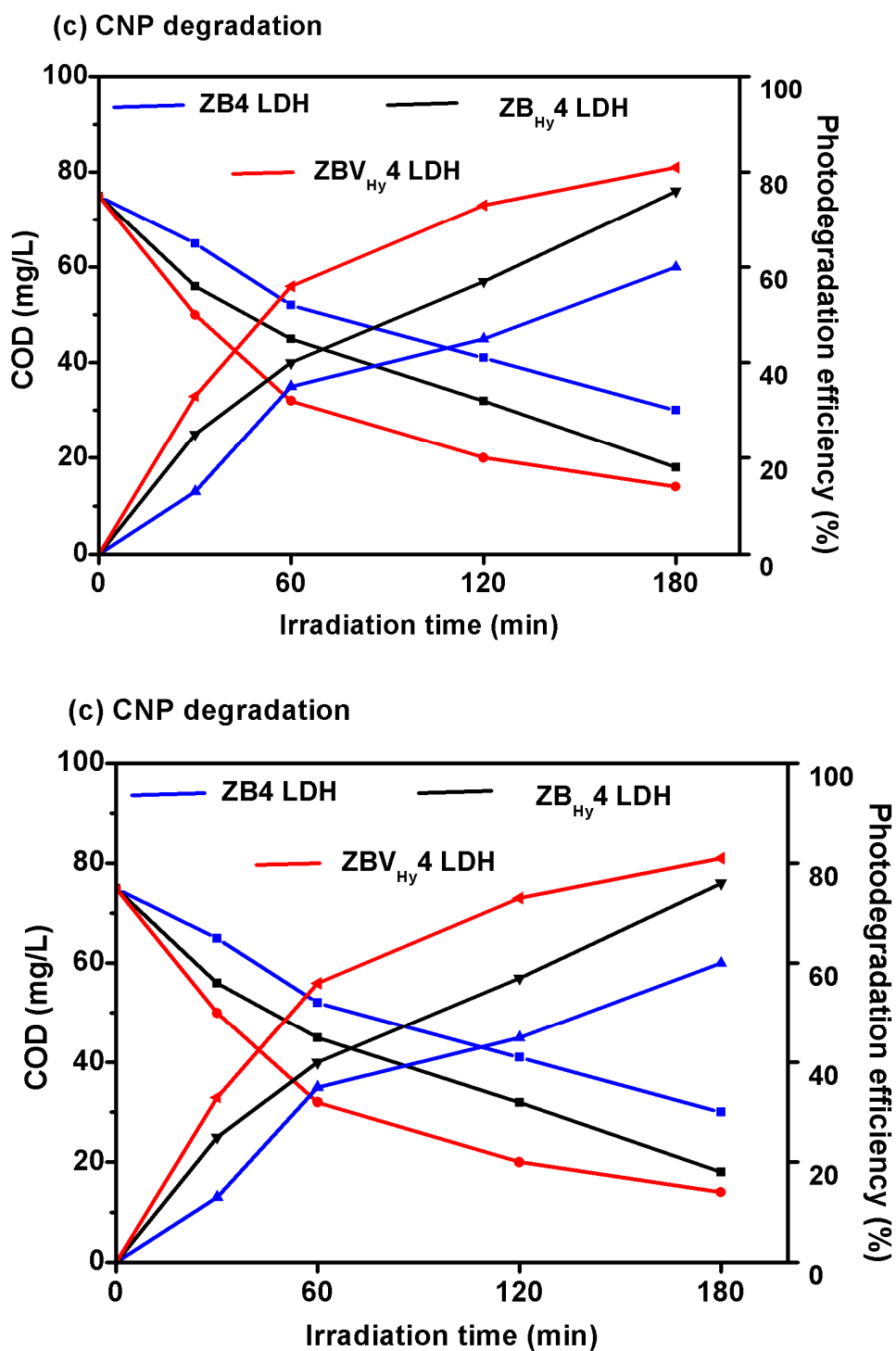


Fig. 8 Photocatalytic degradation of all pollutants (a) MG (b) RHG (c) CNP with ZB4LDH, ZB_{Hy}4 LDH and ZBV_{Hy}4 LDH by COD (mg/L) and photo-degradation efficiency (%).

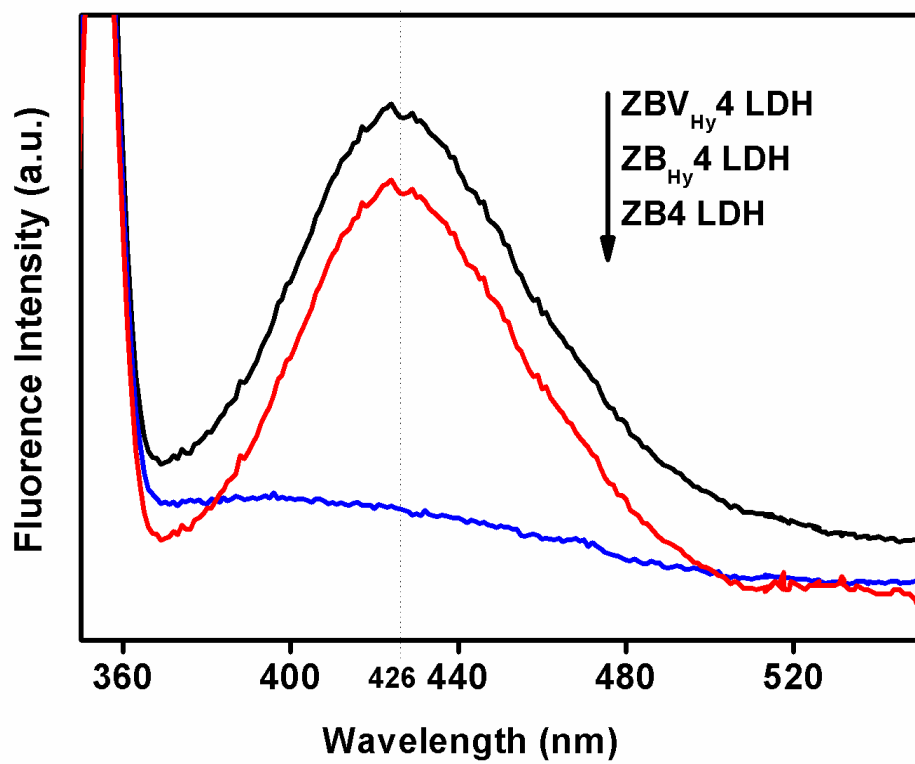


Fig. 9 PL spectral changes with visible-light irradiation time over ZB4LDH, ZB_{Hy}4 LDH and ZBV_{Hy}4 LDH in a 5×10^{-4} M basic solution of terephthalic acid.

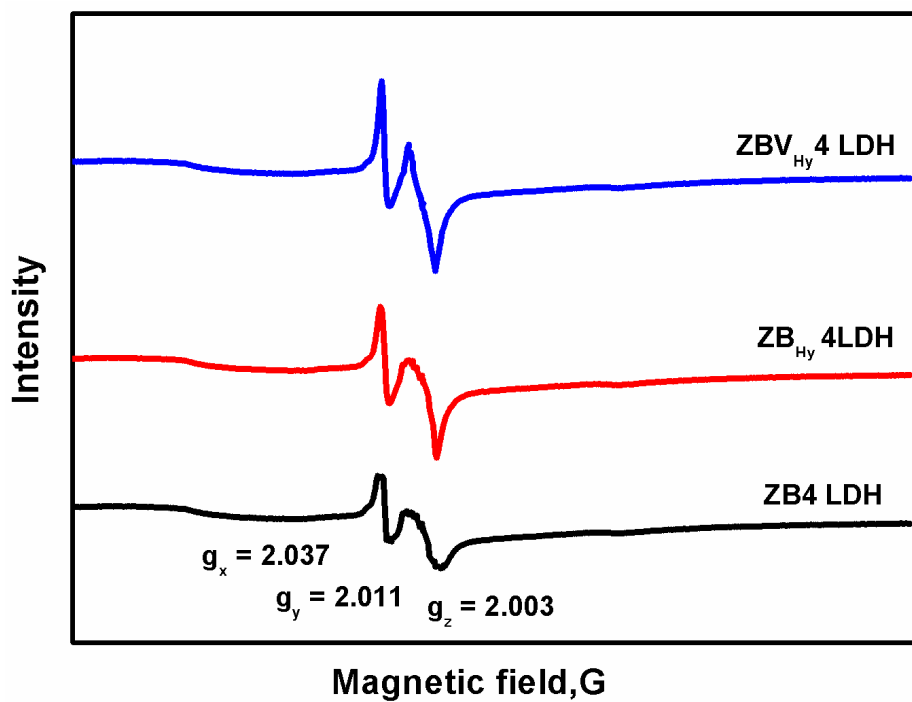


Fig. 10 EPR spectra of ZB4LDH, ZB_{Hy}4 LDH and ZBV_{Hy}4 LDH.